Brücker, C. (2015). Evidence of rare backflow and skin-friction critical points in near-wall turbulence using micropillar imaging. Physics of Fluids, 27(031705), doi: 10.1063/1.4916768

CITY UNIVERSITY LONDON

City Research Online

Evidence of rare backflow and skin-friction critical points in near-wall turbulence using micropillar imaging

Ch. Brücker

Citation: Physics of Fluids (1994-present) **27**, 031705 (2015); doi: 10.1063/1.4916768
View online: http://dx.doi.org/10.1063/1.4916768
View Table of Contents: http://scitation.aip.org/content/aip/journal/pof2/27/3?ver=pdfcov
Published by the AIP Publishing

PHYSICS OF FLUIDS **27**, 031705 (2015)

Evidence of rare backflow and skin-friction critical points in near-wall turbulence using micropillar imaging

Ch. Brücker[a)]
Institute of Mechanics and Fluid Dynamics, TU Bergakademie Freiberg, Freiberg 09599, Germany

(Received 21 December 2014; accepted 20 March 2015; published online 31 March 2015)

The recent discovery of rare backflow events in turbulent boundary layer flows based on the analysis of simulation data has again raised the need of experimental visualizations of wall-shear stress fields in unsteady flows. The localization of critical points, which are thought to strongly correlate with large-scale events in the log-layer, is of importance. Up to now, there is no experimental proof of these rare events and their topological patterns. Their existence in a turbulent boundary-layer flow along a flat plate is shown herein by means of imaging with 2D arrays of flexible micropillars attached at the wall. © *2015 AIP Publishing LLC.* [http://dx.doi.org/10.1063/1.4916768]

The near-wall flow topology in turbulent wall-bounded flows is one of the topics that is still of high interest to understand the complex mutual interaction of events in the log-layer with the near-wall region. The careful analysis of Direct Numerical Simulation (DNS) data of turbulent channel flow by Lanears *et al.*[1] has shown that there are rare events in the near-wall region, where backflow occurs. These seem to occur with a percentage of less than 0.2% within the flow which makes it difficult to capture such events in experimental studies. This might be the reason why some speculation about the existence of near-wall backflow has grown in the past. Only when the DNS data revealed such events, the careful revision of the experimental studies of the authors allowed to indirectly detect such events using point-wise measurements. As soon as backflow is present, it is reasonable to expect that critical points (CPs) (zero wall-shear stress (WSS)) are seen, although not necessarily all regions with negative streamwise WSS need to be CPs. Detailed data were gained recently from highly resolved DNS that allowed to analyze the topology around these CPs in the WSS field (Cardesa *et al.*[2]). The results show a strong correlation between the appearance of CPs and their relation to large-scale events in the log-layer. The overall picture is that a CP marks the tail end of a large-scale structure and it is formed when a vortex at the tail end of the large-scale structure is transported toward the wall. Their extreme nature leads to a long-lasting effect in form of low-streamwise-velocity regions in their "wake" that extend over 800 wall units downstream of a CP. Up to now, however, there is no experimental proof for the existence of such CPs at the wall, and nothing is known about their topological patterns.

Herein, results are shown for micropillar recordings taken in 2011 in an oil flow tunnel installed at Erlangen University, which we re-iterated regarding the existence of such CPs. The flow tunnel was designed for high-resolution optical measurements of transitional and turbulent boundary-layer flow along a flat plate at zero-pressure-gradient (ZPG). The temperature of the working fluid (Odina oil, density $\rho = 840$ kg m^{-3}) and therefore its viscosity could be varied to cover a broader range of Reynolds-numbers in the flow. In this experiment, it was set to room temperature with a kinematic viscosity $\nu = 11 \times 10^{-6}$ m^2/s. A thin flat plate (total length of 3 m) with a sharp trailing edge was placed in the middle of the test section. Different configurations of micropillar arrays distributed over the plate were used at various flow conditions for testing of the sensing capabilities described in Brücker *et al.*[3] Our studies were focused on a region located 1.9 m downstream of the leading edge. At a free stream velocity $U_\infty = 4.2$ m/s, the Reynolds-number based on the streamwise position of the micropillars is

a)Electronic mail: christoph.bruecker@gmx.net

$Re = 7 \times 10^5$; thus, the boundary layer is in an early turbulent state. The Reynolds-number Re_τ defined in terms of the friction velocity $u_\tau = 0.22$ m/s and the flow thickness δ amounts to $\mathrm{Re}_\tau = u_\tau \delta/\nu \approx 940$. The viscous length scale $l_v = \vartheta/u_\tau$ is 50 μm and the non-dimensional viscous time scale is $t^+ = tu_\tau^2/v$. Throughout the paper, the coordinate directions are streamwise (x), spanwise (y), and wall-normal (z) directions. A port with a 2D array of 30×30 flexible filaments on its surface was placed at the predefined location inside the plate such that the port surface was flush with the plate's upper surface. The filaments (diameter $D+ \approx 0.8$, height $L+ \approx 10$, material: Poly-Dimethylsiloxane, $\rho = 1050$ kg/m^3, Young's modulus in the liquid environment $E \approx 1.23 \times 10^6$ N/m^2) extend from the port surface in wall-normal direction into the flow and have a regular spacing of $10x^+$ and 10 y^+. Recordings were taken with a high-speed camera (Photron APX-RS, 1024×1024 px, 1500 fps) with a temporal resolution of 2.93 t^+. Within the viewing field of the camera, a number of 9×9 pillars can be seen. Typically, a total number of 6000 frames were stored on a disc corresponding to a time span of about 17.500 t^+.

In the selected experiments, the micropillar structures were tailored towards higher flexibility such that they bend more easily with the flow than in the previous experiments with structures that bend in the order of the pillar diameter (Brücker,[4] Grosse and Schröder[5]). More flexible sensors have a higher sensitivity as shown in Brücker *et al.*,[6] which is of importance if one is interested in resolving low magnitudes of WSS values in an otherwise turbulent flow where the absolute WSS values can range from zero (CP in the WSS field) to typically three-times the mean, sometimes even five-times the mean, see Örlü and Schlatter.[7] Therefore, high resolution power is especially required near CPs where WSS is zero. Figure 1 illustrates the bending of the filaments (also called "reconfiguration,"

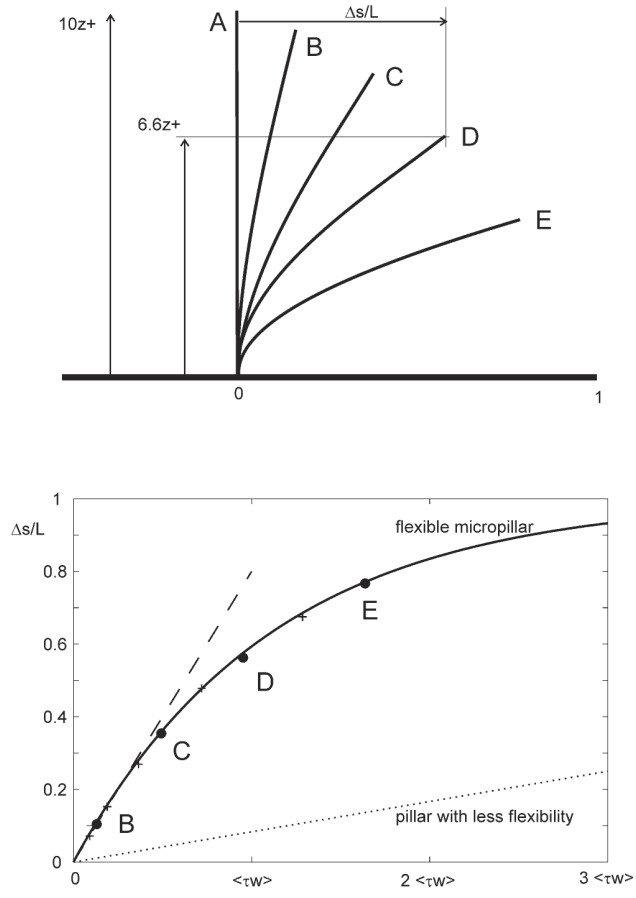

FIG. 1. Reconfiguration of the tailored micropillars in a calibration shear flow (symbols: tip displacement measurements corresponding to the reconfiguration, solid line: curve fit with $\Delta s/L = 1 - \exp(0.018^*\tau)$). A roughly 10-times higher sensitivity (dashed line approximating the linear-elastic range) is achieved at low WSS values compared to a less flexible structure designed for measuring the complete range of WSS in the flow (dotted line representing the linear-elastic behavior over a range of 0–3 times the mean τ_W).

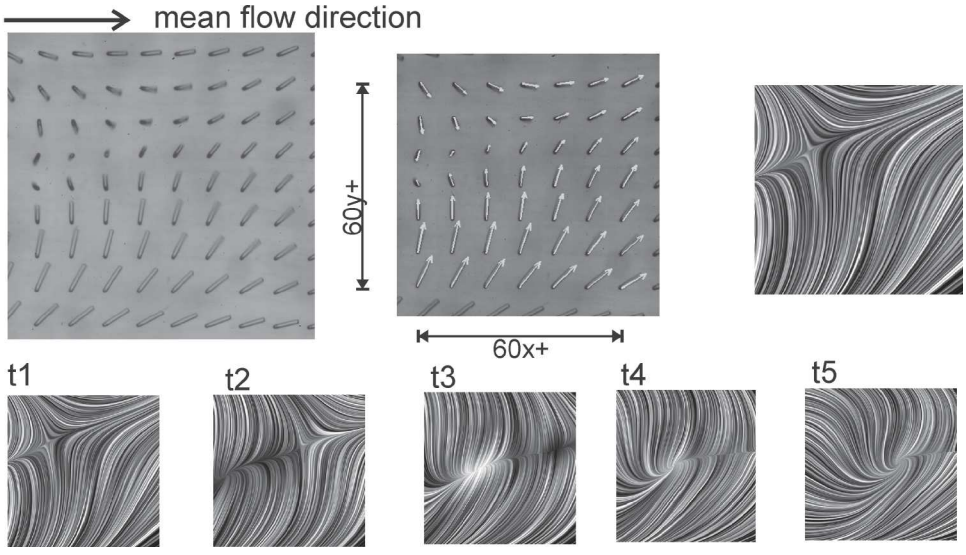

FIG. 2. Evolution of a saddle-node pair (flow is from left to right). Top row, left: original raw image, middle: vectorization of the inner part (7×7 vectors), right: LIC picture generated from the vectorization with cubic interpolation. Bottom row: evolution of topology over 5 successive pictures ($\Delta t^+ = 2.93$). A multimedia file is added for the replay of the original images within a short sequence. (Multimedia view) [URL: http://dx.doi.org/10.1063/1.4916768.1]

compare Vogel[8]) in a shear flow apparatus built for calibration purpose. In the linear-elastic regime (the limit is $\Delta s/L \cong 25\%$, this has also been shown by Paek and Kim[9]), the flexible micropillar shows a 10-times higher sensitivity compared to a less flexible micropillar that is designed to capture the whole span of expected WSS values (dotted line over a span of 0–3 times the mean τ_W). Because of the higher flexibility, the structure bends down with the flow, and for mean flow conditions, the tip is already down to a level $z+ \approx 6.6$, see case D in Figure 1. Hence, although at first one might disqualify such 10+ long filaments as WSS sensors following the design rules given in Brücker *et al.*,[6] they can still remain fully submerged within the viscous sublayer due to their reconfiguration with the flow. On the other hand, as seen in Figure 1 the higher flexibility comes with the disadvantage of increased non-linear behavior at higher WSS when bending of the structures is $\geq 0.5L$. There, the filaments are out of the linear-elastic regime and they increasingly become sensitive to wall-normal velocity fluctuations, too. These regions of large WSS values are not in focus here and the presented recordings do not claim to represent reliable measurements at such levels, see the discussion at the end.

The response of the micropillars is represented by a 2nd order mechanical system of a damped oscillator as derived in Brücker *et al.*[6] The first natural frequency of the filaments in air is 1.2 kHz which was measured in an oscillating flow driven by counter-facing anti-phasic loud-speakers. In the oil bath, damping is higher and the system is overdamped as the quality factor Q = 0.14 is less than 1/sqrt(2), see Eq. (13) in Brücker *et al.*[6] In such an overdamped case, the characteristic time scale is the response time and no resonance exists at all. This response time is the ratio of effective damping to effective spring stiffness as given in Eq. (8) in Brücker *et al.*[6] and is calculated for the present case to be approximately 8.8 t^+. This is expected to be sufficiently high to resolve the relevant WSS fluctuations near the CPs. Based on the DNS results of Cardesa *et al.*,[2] the formation of CP's is linked to large scale events in the buffer layer; thus, the involved frequencies are expected to be lower than the peak frequencies related to the smallest scales in the turbulent flow.

The micropillar bending is given by the evolution of the end-to-end vector in between the base fixation of the filament and the tip position in the extended situation. Measurements with the camera looking from the above onto the wall surface provide only the projection of the end-to-end vector in the wall-parallel x-y-plane $\boldsymbol{Q}$ with its components Qx and Qy. This describes the WSS vector in orientation and magnitude. Following the discussion in Cardesa *et al.*,[2] the local topology of CPs in WSS is given by the similarity invariant of the no-slip tensor A computed at the CP. Within a linear approximation, in the vicinity of the CP (compare Eq. (5) in Ref. 2), the invariant simplifies to

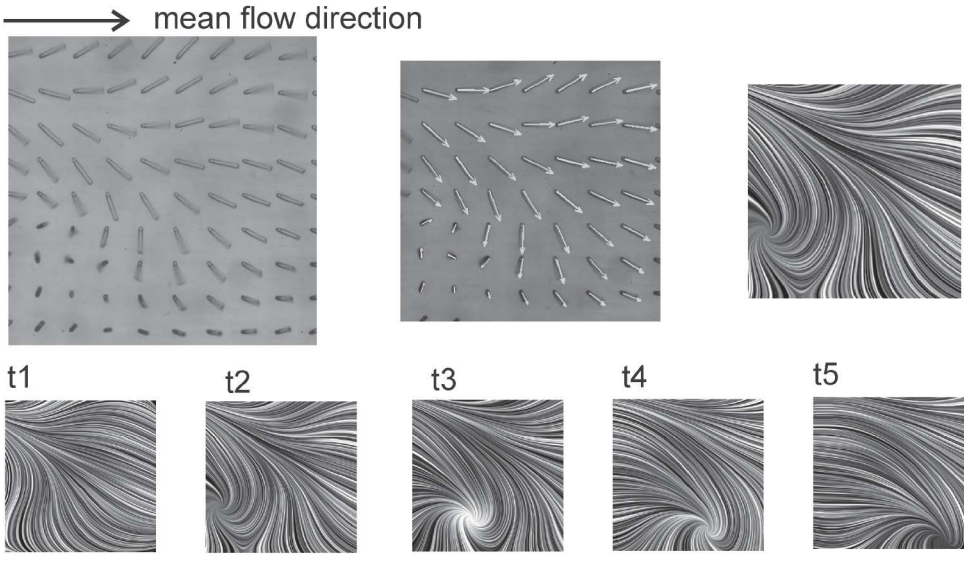

FIG. 3. Evolution of a focus-saddle pair ($\Delta t^+ = 2.93$) in the same recording sequence, for figure caption see Figure 2.

$$p = tr(A) = \mathrm{tr}\left(\begin{bmatrix} \partial^2 u/\partial x\partial z & \partial^2 u/\partial y\partial z \\ \partial^2 v/\partial x\partial z & \partial^2 v/\partial y\partial z \end{bmatrix}\right) \approx \mathrm{tr}\left(\begin{bmatrix} \partial Q_x/\partial x & \partial Q_x/\partial y \\ \partial Q_y/\partial x & \partial Q_y/\partial y \end{bmatrix}\right) = div(\boldsymbol{Q}).$$

Therefore, CPs can be found in our results where the divergence $p = \nabla \cdot \boldsymbol{Q}$, calculated from the Q-vector field on the regular grid by central difference schemes, is large. This criterion was used herein for conditional sampling of the data to exclude phases of low turbulent action from the further analysis as the flow at $Re \approx 7 \times 10^5$ is not in a fully developed turbulent state. Therefore, all time steps were chosen where the average p-value in the field was larger than $2.5p_{rms}$. This left roughly 10% of the total number of images (n = 641) with a high divergence. A typical picture of the flow at a peak value of $p/p_{rms} = 5$ is given in Fig. 2. Note that the raw image is of high contrast, and the filaments are easy to see by the naked eye. A saddle point has appeared on the left side of the image with backflow on its left branch. This structure is transported with a streamwise convection velocity of $U_c^+ \approx 8.5$. In

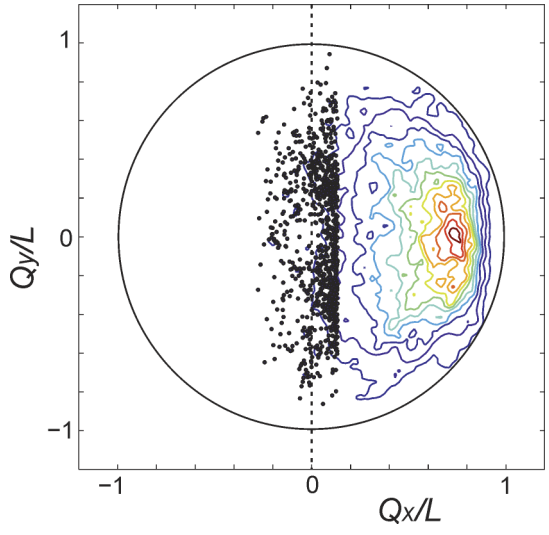

FIG. 4. Contours of 2D distribution of probability density of micropillar configuration vector $\boldsymbol{Q}$ components in the x-y-plane in the turbulent boundary layer (mean streamwise component is $Q_x/L \approx 0.6$). The dots indicate all vectors with the streamwise component Qx/L less than 0.15. Contour lines are calculated from counting the number of vectors in boxes of the size 0.02×0.02. The contour levels are equally spaced in 11 steps.

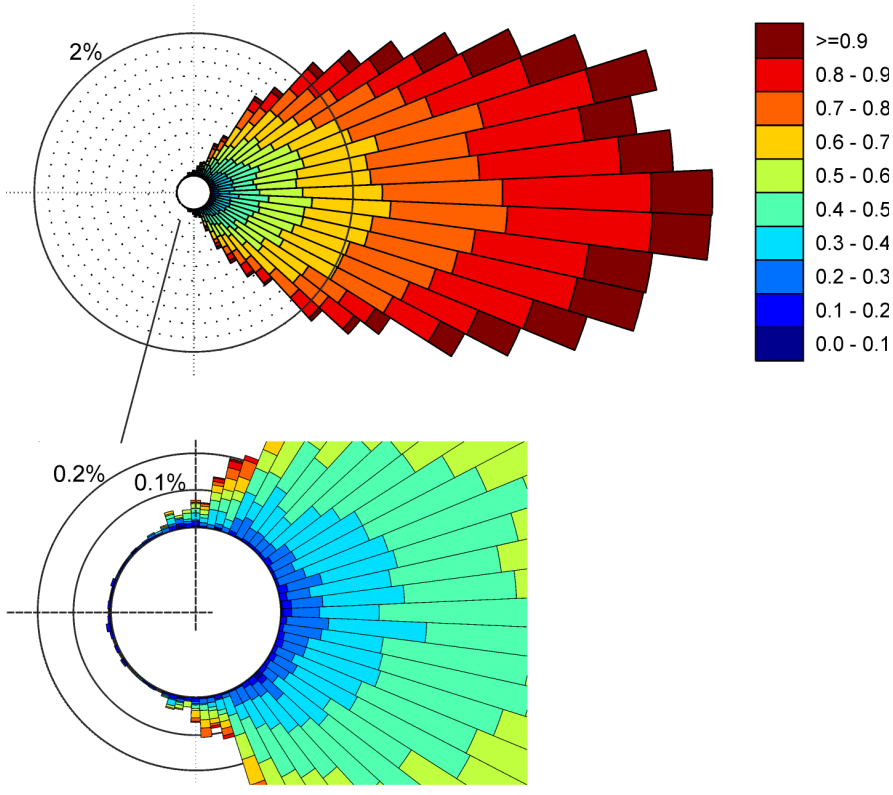

FIG. 5. Probability distribution of the orientation of $\boldsymbol{Q}$ in the x-y-plane (flow is from left to right). The bottom figure shows an enlarged image of the data given above. Angular steps are in 5°. The color indicates the magnitude $|Q|/L$ in the ranges given in the legend bar.

the wake of the saddle, an unstable node is seen in the third image of the sequence. This supports the observation of Cardesa *et al.*[2] that CPs always occur in saddle-node pairs with a certain lifetime. In our results, their connection shows a strong converging flow pattern in spanwise direction, and the node is somewhat lagging the motion of the saddle. Both exist for a time-span of at least $t^+ = 8.8$. In the last image of the sequence, the node seems to transform into a focus. Negative streamwise WSS is now a result of strong curvature of the flow around the CP as seen by the LIC illustration. This strong tilt of the WSS vectors against the mean-flow direction leads us to conclude that the underlying structures in the buffer layers are large ones, however, in no case bypass rollers that might still exist in the flow as reminders of the transition process. Otherwise, a stronger coherence in spanwise direction should be present, which is not seen.

Figure 3 illustrates another example of a pair of CPs in form of a focus-saddle pair. Note that the streamwise backflow here also stems from regions of higher WSS where the angle of the Q-vectors relative to the streamwise direction exceeds 90°. Thus, such rare backflow events are not only born from regions of low magnitude WSS but they are also generated from larger WSS vectors that have a strong tilt against the streamwise direction. Apparently, the backflow region is located in areas of high spanwise gradients of the WSS, i.e., in the center between a WSS-cell with strong positive streamwise WSS pointing to the lower right and a WSS-cell with low magnitude located in the left corner. The cell with high magnitude of WSS also shows a larger divergence of the Q-vectors along a dividing streamline pointing from the upper left corner to the lower right of the field. This line is where the flow spreads out into both directions laterally away. This suggests a strong fluid motion towards the wall, presumably a footprint of strong down-wash. Such extreme wall-normal velocity events were found in the neighborhood of CP's as documented by Lenaers *et al.*[1] Again, the convection velocity of the structure is roughly the same as observed above.

From all conditional sampled data, the JPDF of streamwise and spanwise component of $\boldsymbol{Q}$ was plotted in Fig. 4. The vectors are normalized with the length L. Note that the JPDF in the higher

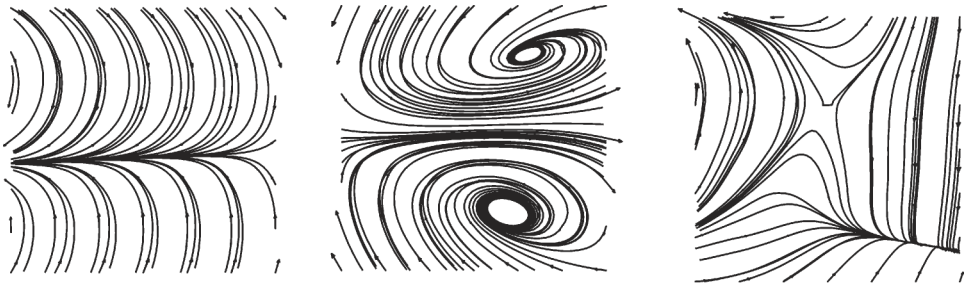

FIG. 6. Results of a snapshot POD of the fluctuating Q-field. Here, the first three antisymmetric modes are shown in order from left to right. The arrows indicate the flow direction that can be positive or negative in reversed form.

WSS-regions is much skewed towards the mean as expected from the non-linear behavior shown in Figure 1. These regions however are not within the focus herein. To highlight the nature of possible backflow events, all vectors where the streamwise bending component is $Q_x/L < 0.15$ were plotted as dots. The results indicate that the events with negative streamwise WSS are not only distributed in regions of low WSS but also stem from regions where the spanwise component is of considerable magnitude. Thus, events with strong spanwise WSS seem to correlate with such negative streamwise backflow as a consequence of strong curvature of fluid motion in the wall-parallel plane.

This conclusion is supported by the angular distribution of $\boldsymbol{Q}$ shown in Fig. 5. Regions with streamwise backflow components are found more often in the arc from ±90° to 115° than at angles larger than ±115°. Note that such vectors appear in less than 0.1% of the number of the conditional samples. The accumulated number of vectors with an orientation larger than ±90° in the complete sequence is about 0.05%; thus, these events are extremely rare as found in the DNS data, too. A possible correlation between the WSS magnitude and angle for $Qx/L < 0.15$ is not clearly seen in Fig. 4, but the distribution shown in Figure 5 shows the tendency of lower magnitude with increasing angle in the arc >±90°.

A further analysis applies the proper orthogonal decomposition (snapshot POD) technique to the fluctuating field of Q-$\langle Q \rangle$ within the conditional sampled dataset. The first three antisymmetric modes φ1, φ2, φ3 are given in Fig. 6. Mode φ1 shows a spanwise flow with converging (alternative diverging) character centered to the midline, mode φ2 reveals a pair of counter-rotating foci, and mode φ3 represents a saddle. The first non-symmetric mode ψ1 (not shown here) resembles mode φ1 in energy and pattern except that the line of symmetry is located off-center. The same holds for the non-symmetric mode ψ2 in comparison to mode φ2. Therefore, the modes shown in Figure 6 represent fundamental modes in such a way that we can interpret those as centered to the field of view. When comparing the patterns in Fig. 6 with the conditionally averaged fields of WSS from DNS data by Cardesa *et al.*,[2] it is obvious that our results correlate to certain regions around the CPs in their simulation results. Mode φ1, the one with the highest energy, correlates with the long tail of streamwise streaks of negative and positive spanwise WSS centered with $\Delta x_2 = 0$ in Fig. 10(b) in Ref. 2. Since this is a long-lasting structure in the wake of the CP, it is a pattern of high energy in our POD results. The second mode φ2 with the two counter-rotating foci generates a divergent-convergent pattern in spanwise WSS around the center. This corresponds to the region around the CP in Fig. 10(a) in Ref. 2 where streamwise WSS is reduced, but spanwise WSS reaches maximum values. Even the spacing of antisymmetric peaks in spanwise WSS at a value of $60\Delta x_2$ in Ref. 2 is comparable to the spanwise spacing of the foci measured to about 50 y^+ in our experiment.

The direct imaging of the WSS topology near CPs using micropillar imaging in near-wall turbulence shows striking similarities with the recent high-resolution details gained from the DNS data reported in Ref. 2, although the experiments were run at lower Reynolds-numbers at $Re_\tau \approx 940$. The extreme rarity of the backflow events observed in DNS of channel flows reported in Ref. 1 has been proven to hold also in turbulent boundary layer flows at ZPG as shown herein. Those backflow events occur in our experiments at about 0.05% of the recorded images and are always linked to CPs. There is a preference of these backflow regions with WSS vectors that are strongly tilted against the streamwise direction in angles between 90° and 115°.

A necessary condition for the detection of such events with sufficient spatial resolution in the array of sensors was tailoring the sensitivity of the pillars to low WSS values in an otherwise turbulent flow, where the WSS magnitude spans a wide range. Thus, the structures were made more flexible at the expense of losing accuracy at WSS values in the higher range. Therefore, the recorded patterns are of rather qualitative nature; one may understand those as visualizations analogue to the Schlieren visualizations in compressible flows. On the other hand, detecting the topological pattern near a CP requires sufficient resolution power of the sensors against the measurement uncertainty which cannot be achieved in arrays with sensors tuned to capture the full range of WSS levels. Therefore, such events of weak near-wall backflow may have been overlooked so far, which is where we see the benefit of the tailored structures. The evidence is provided herein for a certain phenomenon that was looked for and where the sensors were tailored for, while for other applications or phenomena the significant uncertainty associated with larger bending may disqualify a physical interpretation. A possible practical solution for the resolution problem could be to simultaneously use structures of different effective stiffness next to each other to cover different dynamic ranges with comparable accuracy. However, it is difficult to prevent flow disturbance and mutual interaction if a number of sensors with different sensitivities are placed close to each other. Another possible solution is the use of channeling optics as proposed by the author in another communication, which allows focusing simultaneously on a large number of individual sensors with high resolution in each channel. Nonetheless, such a solution was not available when we took the recordings back in 2011.

Finally, the hitherto agreed upon limit for the length of micropillar sensors for quantitative WSS measurements, i.e., the classical 5z+ definition for the thickness of the viscous sublayer, possibly needs some revision in the context described herein. This definition of the viscous sublayer is linked to the local mean, still measurements may focus on WSS levels far away from the mean, an example thereof given herein for the lower range near CP's in the WSS field. The existing DNS data from Cardesa *et al.*[2] may help to analyze in the region around a CP how far away from the wall ($\leq$10z+) the linear approximation of the no-slip tensor still is valid, possibly beyond the classical 5z+ definition. Therefore, DNS coupled with simulations on the load profile on such filaments in the WSS field may give a definite answer about the measurement precision in such conditions.

This material is based upon the work supported by the Air Force Office of Scientific Research, Air Force Material Command, USAF under Award No. FA9550-14-1-0315 and program manager Gregg Abate. The measurements in the Erlangen oil channel were made possible by the support of the DFG and the LSTM which is gratefully acknowledged here.

[1] P. Lenaers, Q. Li, G. Brethouwer, P. Schlatter, and R. Örlü, "Rare backflow and extreme wall-normal velocity fluctuations in near-wall turbulence," Phys. Fluids **24**, 035110 (2012).
[2] J. Cardesa, J. Monty, J. Soria, and M. Chong, "Skin-friction critical points in wall-bounded flows," J. Phys.: Conf. Ser. **506**, 012009 (2014).
[3] C. Brücker, J. Spatz, and W. Schröder, "Feasibility of wall shear stress imaging using micro structured surfaces with flexible micropillars," Exp. Fluids **39**(2), 464-474 (2005).
[4] C. Brücker, "Signature of varicose wave packets in the viscous sublayer," Phys. Fluids **20**, 061701 (2008).
[5] S. Grosse and W. Schröder, "Wall-shear stress patterns of coherent structures in turbulent duct flow," J. Fluid Mech. **633**, 147-158 (2009).
[6] C. Brücker, D. Bauer, and H. Chaves, "Dynamic response of micro-pillar sensors measuring fluctuating wall-shear-stress," Exp. Fluids **42**, 737-749 (2007).
[7] R. Örlü and P. Schlatter, "On the fluctuating wall-shear stress in zero-pressure-gradient turbulent boundary layers," Phys. Fluids **23**, 021704 (2011).
[8] S. Vogel, "Drag and reconfiguration of broad leaves in high winds," J. Exp. Bot. **40**, 941-948 (1989).
[9] J. Paek and J. Kim, "Microsphere-assisted fabrication of high aspect-ratio elastomeric micropillars and waveguides," Nat. Commun. **5**, 3324 (2014).